characteristics, and demonstrate the difference between those of the co- and cross-polarizations. We also propose the Cauchy distribution as the best-fit to model the Doppler frequency spectrum. An analysis of the shape-dependency of this model provides comparable results to those of the Doppler spread.

Future work includes an enhancement of the COST 2100 channel model [2] with Doppler characteristics for user motion, and an evaluation of the effect of antenna deembedding.

REFERENCES

[1] I. R. Capoglu, Y. Li, and A. Swami, "Effect of Doppler spread in OFDM-based UWB systems," *IEEE Trans. Wireless Commun.*, vol. 4, no. 5, pp. 2559–2567, Sep. 2005.

[2] R. Verdone and A. Zanella, "Pervasive mobile and ambient wireless communications: COST action 2100," in *Signals and Communication Technology*. New York, NY, USA: Springer, 2012.

[3] A Domazetovic, L. J. Greenstein, N. B. Mandayam, and I Seskar, "Estimating the Doppler spectrum of a short-range fixed wireless channel," *IEEE Commun. Lett.*, vol. 7, no. 5, pp. 227–229, May 2003.

[4] P. Pagani and P. Pajusco, "Characterization and modeling of temporal variations on an ultrawideband radio link," *IEEE Trans. Antennas Propag.*, vol. 54, no. 11, pp. 3198–3206, Nov. 2006.

[5] H. P. Bui, H. Nishimoto, Y. Ogawa, T. Nishimura, and T. Ohgane, "Channel characteristics and performance of MIMO E-SDM systems in an indoor time-varying fading environment," *EURASIP J. Wireless Commun. Netw.*, vol. 44, pp. 1–13, 2010.

[6] M. Herdin, N. Czink, H. Ozcelik, and E. Bonek, "Correlation matrix distance: A meaningful measure for evaluation of non-stationary MIMO channels," in *Proc. IEEE Veh. Technol. Conf.*, 1005, pp. 136–140.

[7] L. Bernadó, "Non-stationarity in vehicular wireless channels," Ph.D. dissertation, Technische Universität Wien, Vienna, Austria, 2012.

Error Bound of the Multilevel Adaptive Cross Approximation (MLACA)

Xinlei Chen, Changqing Gu, Alex Heldring, Zhuo Li, and Qunsheng Cao

***Abstract*—An error bound of the multilevel adaptive cross approximation (MLACA), which is a multilevel version of the adaptive cross approximation-singular value decomposition (ACA-SVD), is rigorously derived. For compressing an off-diagonal submatrix of the method of moments (MoM) impedance matrix with a binary tree, the L-level MLACA includes $L+1$ steps, and each step includes 2^L ACA-SVD decompositions. If the relative Frobenius norm error of the ACA-SVD used in the MLACA is smaller than ε, the rigorous proof in this communication shows that the relative Frobenius norm error of the L-level MLACA is smaller than $(1+\varepsilon)^{L+1}-1$. In practical applications, the error bound of the MLACA can be approximated as $\varepsilon(L+1)$, because ε is always $\ll 1$. The error upper bound can be used to control the accuracy of the MLACA. To ensure an error of the L-level MLACA smaller than ε for different L, the ACA-SVD threshold can be set to $(1+\varepsilon)^{\frac{1}{L+1}}-1$, which approximately equals $\varepsilon/(L+1)$ for practical applications.**

***Index Terms*—Error bound, low-rank decomposition, method of moments (MoM), multilevel adaptive cross approximation (MLACA).**

I. INTRODUCTION

Adaptive cross approximation (ACA)-based algorithms [1]–[9] become more and more popular in solving the method of moments (MoM) [10] impedance matrix equations obtained from discretizing integral equations due to their efficient, adaptive, and kernel-independent properties. These algorithms can adaptively and efficiently compress the rank-deficient impedance submatrix related to two well-separated blocks into a product of matrices requiring much less memory. As a result, the computational time and storage cost of the MoM can be significantly decreased.

The conventional ACA algorithm [1], [2] can reduce the computational time and memory requirement of the MoM to $O(N^{4/3}\log N)$ [2] for analyzing moderate electrical size targets with iterative solvers, where N is the number of unknowns. However, for very large targets, the complexities of the conventional ACA become as high as $O(N^3)$ and $O(N^2)$ [2] for CPU time and storage, respectively. The ACA-singular value decomposition (ACA-SVD) [3], [4] can optimize the storage of the ACA by transforming the ACA decomposition into a truncated SVD. Nevertheless, the ACA-SVD does not improve the

Manuscript received July 23, 2015; revised November 01, 2015; accepted November 14, 2015. Date of publication November 20, 2015; date of current version December 31, 2015. This work was supported in part by the National Nature Science Foundation of China under Grant 61501227 and Grant 61071019, in part by the Postdoctoral Science Foundation of China under Grant 2015M581789, in part by the Fundamental Research Funds for the Central Universities under Grant NJ20140009, and in part by the Priority Academic Program Development of Jiangsu Higher Education Institutions.

X. Chen, C. Gu, Z. Li, and Q. Cao are with the Key Laboratory of Radar Imaging and Microwave Photonics, Ministry of Education, College of Electronic and Information Engineering, Nanjing University of Aeronautics and Astronautics, Nanjing, China (e-mail: chenxl@nuaa.edu.cn; gucq@nuaa.edu.cn).

A. Heldring is with the Antenna Laboratory, Department of Signal Processing and Telecommunications, Universitat Politècnica de Catalunya, 08034 Barcelona, Spain (e-mail: heldring@tsc.upc.edu).

Color versions of one or more of the figures in this communication are available online at http://ieeexplore.ieee.org.

Digital Object Identifier 10.1109/TAP.2015.2502624

asymptotic complexity of the conventional ACA. To mitigate this problem, the multilevel ACA (MLACA) [5] has been proposed, which is a multilevel version of the ACA-SVD with the aid of the butterfly algorithm [11]. As a result, it can achieve $O(N^2)$ computational complexity and $O(N\log^2 N)$ storage complexity for very large targets [5].

For compressing an off-diagonal submatrix of the MoM impedance matrix, in the single-level ACA-SVD algorithm, the ACA-SVD decomposition [3], [4] of the impedance submatrix is directly performed. The decomposition error can be easily estimated, as the threshold of the used ACA-SVD. Different from the single-level ACA-SVD algorithm, the L-level MLACA [5] algorithm includes $L+1$ steps, and each step involves 2^L ACA-SVD decompositions if a binary tree is used to partition the target under analysis. Since there are $2^L(L+1)$ ACA-SVD decompositions in the L-level MLACA, a question is raised here: how large does the error of the MLACA become? In [5], the authors intuitively reason that the maximum error of the L-level MLACA in the worst case does not exceed $\varepsilon(L+2)$, where ε is the error of the ACA-SVD used in the MLACA. However, a rigorous derivation of this conclusion is not provided in [5]. In this communication, an upper bound of the relative Frobenius norm [12] error of the MLACA is rigorously derived. The proof shows that the relative Frobenius norm error of the L-level MLACA is smaller than $(1+\varepsilon)^{L+1}-1$ when the relative Frobenius norm error of the ACA-SVD is smaller than ε. The error bound of the MLACA can be approximated as $\varepsilon(L+1)$, because ε is always $\ll 1$ in practical applications. Consequently, the threshold of the ACA-SVD can be set to $(1+\varepsilon)^{\frac{1}{L+1}}-1 \approx \varepsilon/(L+1)$ to ensure an error of the L-level MLACA below ε for various L.

II. Formulations

First, the MLACA algorithm is briefly illustrated in Section II-A. Then, in Section II-B, two inequalities and one equality are proved, which are used in the derivation of the error bound of the MLACA. Finally, the bound of the relative Frobenius norm error of the MLACA is derived in detail in Section II-C.

A. Multilevel Adaptive Cross Approximation

To apply the MLACA algorithm [5] on the MoM impedance matrix, the geometry of the target under analysis needs to be split hierarchically into blocks at different levels. As in [5], the binary tree is employed here. The impedance submatrices associated with well-separated blocks at the peer level can be efficiently compressed by the MLACA.

We assume that the target is divided into l' levels by the binary tree, where level l' is the finest level, and consider the MoM impedance submatrix $\mathbf{B}^{(0)}$ representing the interactions of the basis functions in two well-separated blocks at level l. The L-level MLACA can be used to compress $\mathbf{B}^{(0)}$. It contains $L+1$ steps, where $L=l'-l$. At the pth step ($0 \le p \le L$), the rows of $\mathbf{B}^{(p)}$ are first joined according to the partitioning at level $l'-p$, and then the columns of $\mathbf{B}^{(p)}$ are split according to the partitioning at level $l+p$. This operation identifies a total of 2^L new submatrices $\hat{\mathbf{B}}_i^{(p)}$ ($i=1,2,3,\ldots,2^L$) that are compressed into $\mathbf{A}_i^{(p+1)}\mathbf{B}_i^{(p+1)}$ by the ACA-SVD [3], [4], [9], as shown in Fig. 1. Then, $\mathbf{B}^{(p)}$ can be approximated with

$$\mathbf{B}^{(p)} \approx \mathbf{A}^{(p+1)}\mathbf{B}^{(p+1)} \tag{1}$$

where $\mathbf{A}^{(p+1)}$ is composed of the left singular vectors of the $\hat{\mathbf{B}}_i^{(p)}$ and $\mathbf{B}^{(p+1)}$ includes the products of the singular values and the right singular vectors of the $\hat{\mathbf{B}}_i^{(p)}$. When all $L+1$ steps of the MLACA are completed, $\mathbf{B}^{(0)}$ is compressed into a product of $L+2$ sparse matrices as follows:

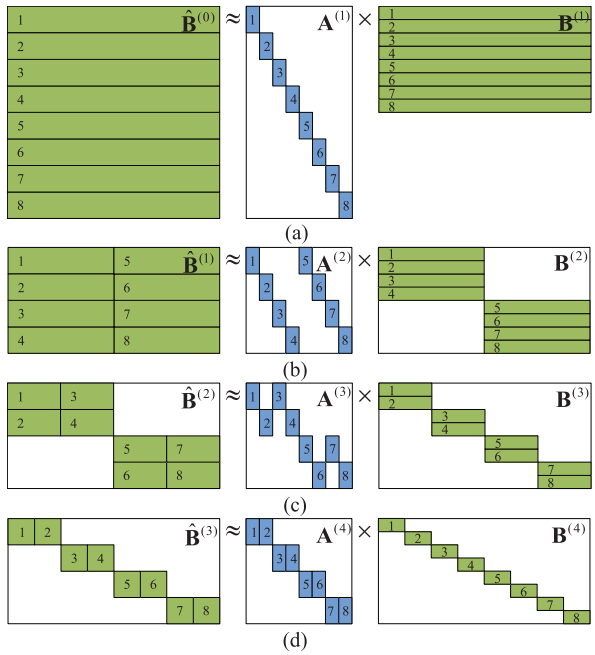

Fig. 1. Pictorial representation of the three-level MLACA. (a) Step 0. (b) Step 1. (c) Step 2. (d) Step 3.

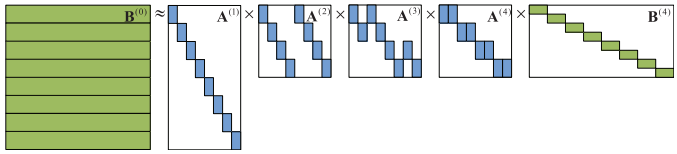

Fig. 2. $\mathbf{B}^{(0)}$ is compressed into the product of $\mathbf{A}^{(1)}\mathbf{A}^{(2)}\mathbf{A}^{(3)}\mathbf{A}^{(4)}\mathbf{B}^{(4)}$ by the three-level MLACA.

$$\mathbf{B}^{(0)} \approx \mathbf{A}^{(1)}\mathbf{A}^{(2)}\mathbf{A}^{(3)}\cdots\mathbf{A}^{(L+1)}\mathbf{B}^{(L+1)} = \left(\prod_{p=1}^{L+1}\mathbf{A}^{(p)}\right)\mathbf{B}^{(L+1)} \tag{2}$$

where $\mathbf{A}^{(p)}$ for $1 \le p \le (L+1)$ and $\mathbf{B}^{(L+1)}$ have 2^L submatrices. All the submatrices of $\mathbf{A}^{(p)}$ are orthogonal matrices.

Fig. 1 shows the pictorial representation of the compression process of $\mathbf{B}^{(0)}$ by the three-level MLACA. Finally, $\mathbf{B}^{(0)}$ is decomposed into the product of $\mathbf{A}^{(1)}\mathbf{A}^{(2)}\mathbf{A}^{(3)}\mathbf{A}^{(4)}\mathbf{B}^{(4)}$ as shown in Fig. 2.

Assuming that the relative Frobenius norm error of the ACA-SVD used in the MLACA is not larger than ε, the purpose of this communication is to give an upper bound of the relative error (3) of the MLACA for compressing $\mathbf{B}^{(0)}$

$$\frac{\left\|\mathbf{B}^{(0)} - \left(\prod_{p=1}^{L+1}\mathbf{A}^{(p)}\right)\mathbf{B}^{(L+1)}\right\|_F}{\left\|\mathbf{B}^{(0)}\right\|_F} \tag{3}$$

where $\|\cdot\|_F$ stands for the Frobenius norm [12]. The Frobenius norm of $\mathbf{D} \in \mathbb{C}^{m\times n}$ is defined as

$$\|\mathbf{D}\|_F = \sqrt{\sum_{i=1}^{m}\sum_{j=1}^{n}|d_{ij}|^2} \tag{4}$$

where d_{ij} is the element in the ith row and jth column of $\mathbf{D}$.

B. Lemmas

In this section, we prove three lemmas that we need for the MLACA error upper bound derived in the next section.

Lemma 1: $\left\|\mathbf{B}^{(p)}-\mathbf{A}^{(p+1)}\mathbf{B}^{(p+1)}\right\|_F \le \varepsilon\left\|\mathbf{B}^{(p)}\right\|_F$ *for* $0 \le p \le L$.

Proof: At the pth step of the MLACA [5] for $0 \le p \le L$, the ith submatrix of $\hat{\mathbf{B}}^{(p)}$, $\hat{\mathbf{B}}_i^{(p)}$, for $i = 1, 2, 3, \ldots, 2^L$ is compressed by the truncated ACA-SVD [3], [4], [9] into

$$\hat{\mathbf{B}}_i^{(p)} \approx \mathbf{U}_i^{(p)}\mathbf{S}_i^{(p)}\mathbf{V}_i^{(p)} \tag{5}$$

where $\mathbf{U}_i^{(p)}$ is the truncated left singular matrix of $\hat{\mathbf{B}}_i^{(p)}$, $\mathbf{V}_i^{(p)}$ is the truncated right singular matrix of $\hat{\mathbf{B}}_i^{(p)}$, and $\mathbf{S}_i^{(p)}$ is a diagonal matrix and contains the retained singular values of $\hat{\mathbf{B}}_i^{(p)}$. $\mathbf{U}_i^{(p)}$ and $\mathbf{V}_i^{(p)}$ are orthogonal matrices.

We recall that we assume the relative Frobenius norm error of (5) to be smaller than ε, thus

$$\frac{\left\|\hat{\mathbf{B}}_i^{(p)}-\mathbf{U}_i^{(p)}\mathbf{S}_i^{(p)}\mathbf{V}_i^{(p)}\right\|_F}{\left\|\hat{\mathbf{B}}_i^{(p)}\right\|_F} \le \varepsilon. \tag{6}$$

Then, we have

$$\left\|\hat{\mathbf{B}}_i^{(p)}-\mathbf{A}_i^{(p+1)}\mathbf{B}_i^{(p+1)}\right\|_F \le \varepsilon\left\|\hat{\mathbf{B}}_i^{(p)}\right\|_F \tag{7}$$

where $\mathbf{A}_i^{(p+1)}$ and $\mathbf{B}_i^{(p+1)}$ denote the ith submatrix of $\mathbf{A}^{(p+1)}$ and $\mathbf{B}^{(p+1)}$, respectively

$$\mathbf{A}_i^{(p+1)} = \mathbf{U}_i^{(p)} \tag{8}$$

$$\mathbf{B}_i^{(p+1)} = \mathbf{S}_i^{(p)}\mathbf{V}_i^{(p)}. \tag{9}$$

According to the definition of the Frobenius norm [12], the square of the Frobenius norm of a matrix equals the sum of the squares of the Frobenius norm of its submatrices. Thus

$$\left\|\hat{\mathbf{B}}^{(p)}-\mathbf{A}^{(p+1)}\mathbf{B}^{(p+1)}\right\|_F^2 = \sum_{i=1}^{2^L}\left\|\hat{\mathbf{B}}_i^{(p)}-\mathbf{A}_i^{(p+1)}\mathbf{B}_i^{(p+1)}\right\|_F^2. \tag{10}$$

Substituting (7) into (10) yields

$$\left\|\hat{\mathbf{B}}^{(p)}-\mathbf{A}^{(p+1)}\mathbf{B}^{(p+1)}\right\|_F^2 \le \varepsilon^2\sum_{i=1}^{2^L}\left\|\hat{\mathbf{B}}_i^{(p)}\right\|_F^2 = \varepsilon^2\left\|\hat{\mathbf{B}}^{(p)}\right\|_F^2. \tag{11}$$

Taking the square root of both sides of (11), we find

$$\left\|\mathbf{B}^{(p)}-\mathbf{A}^{(p+1)}\mathbf{B}^{(p+1)}\right\|_F \le \varepsilon\left\|\mathbf{B}^{(p)}\right\|_F \tag{12}$$

where it has been used that $\hat{\mathbf{B}}^{(p)} = \mathbf{B}^{(p)}$.

Lemma 1 states that if the relative Frobenius norm error of the truncated ACA-SVD is smaller than ε, the relative Frobenius norm error of the pth step in the MLACA is also bounded by ε.

Lemma 2: $\left\|\mathbf{A}^{(p)}\mathbf{B}^{(p)}\right\|_F = \left\|\mathbf{B}^{(p)}\right\|_F$ *for* $1 \le p \le (L+1)$.

Proof: The square of $\left\|\mathbf{A}^{(p)}\mathbf{B}^{(p)}\right\|_F$ can be rewritten as

$$\left\|\mathbf{A}^{(p)}\mathbf{B}^{(p)}\right\|_F^2 = \sum_{i=1}^{2^L}\left\|\mathbf{A}_i^{(p)}\mathbf{B}_i^{(p)}\right\|_F^2. \tag{13}$$

Because $\mathbf{A}_i^{(p)}$ is orthogonal for $i = 1, 2, 3, \ldots, 2^L$, due to the orthogonal invariance of the Frobenius norm [12], we have

$$\left\|\mathbf{A}_i^{(p)}\mathbf{B}_i^{(p)}\right\|_F = \left\|\mathbf{B}_i^{(p)}\right\|_F. \tag{14}$$

Substituting (14) into (13), we obtain

$$\left\|\mathbf{A}^{(p)}\mathbf{B}^{(p)}\right\|_F^2 = \sum_{i=1}^{2^L}\left\|\mathbf{B}_i^{(p)}\right\|_F^2 = \left\|\mathbf{B}^{(p)}\right\|_F^2. \tag{15}$$

Taking the square root of both sides of (15), we have

$$\left\|\mathbf{A}^{(p)}\mathbf{B}^{(p)}\right\|_F = \left\|\mathbf{B}^{(p)}\right\|_F. \tag{16}$$

Lemma 2 asserts that $\mathbf{A}^{(p)}$ does not change the Frobenius norm of $\mathbf{B}^{(p)}$ when multiplying $\mathbf{B}^{(p)}$ by $\mathbf{A}^{(p)}$, even though $\mathbf{A}^{(p)}$ is not an orthogonal matrix in general.

Furthermore, Lemma 2 implies:

Corollary 1:

$$\left\|\mathbf{A}^{(p)}\mathbf{M}\right\|_F = \|\mathbf{M}\|_F \tag{17}$$

if the matrix $\mathbf{M}$ has the same sparsity pattern as $\mathbf{B}^{(p)}$.

Lemma 3: $\left\|\mathbf{B}^{(p+1)}\right\|_F / \left\|\mathbf{B}^{(p)}\right\|_F \le 1+\varepsilon$ for $0 \le p \le L$.

Proof: $\left\|\mathbf{A}^{(p+1)}\mathbf{B}^{(p+1)}\right\|_F$ can be rewritten as

$$\left\|\mathbf{A}^{(p+1)}\mathbf{B}^{(p+1)}\right\|_F = \left\|\mathbf{B}^{(p)}-\mathbf{A}^{(p+1)}\mathbf{B}^{(p+1)}-\mathbf{B}^{(p)}\right\|_F. \tag{18}$$

Due to the triangle inequality of a matrix norm [12], we have

$$\left\|\mathbf{A}^{(p+1)}\mathbf{B}^{(p+1)}\right\|_F \le \left\|\mathbf{B}^{(p)}-\mathbf{A}^{(p+1)}\mathbf{B}^{(p+1)}\right\|_F + \left\|\mathbf{B}^{(p)}\right\|_F. \tag{19}$$

With Lemmas 1 and 2, this leads to

$$\left\|\mathbf{B}^{(p+1)}\right\|_F \le \varepsilon\left\|\mathbf{B}^{(p)}\right\|_F + \left\|\mathbf{B}^{(p)}\right\|_F. \tag{20}$$

Or equivalently

$$\frac{\left\|\mathbf{B}^{(p+1)}\right\|_F}{\|\mathbf{B}^{(p)}\|_F} \le 1+\varepsilon. \tag{21}$$

C. Error Bound of MLACA

In this section, the Frobenius norm error bound of the MLACA is derived in detail. First, the numerator of (3) is considered, which can be rewritten as

$$\begin{aligned}
&\left\|\mathbf{B}^{(0)}-\left(\prod_{p=1}^{L+1}\mathbf{A}^{(p)}\right)\mathbf{B}^{(L+1)}\right\|_F \\
&= \left\|\mathbf{B}^{(0)}+\sum_{p=1}^{L}\left(\left(\prod_{q=1}^{p}\mathbf{A}^{(q)}\right)\mathbf{B}^{(p)}-\left(\prod_{q=1}^{p}\mathbf{A}^{(q)}\right)\mathbf{B}^{(p)}\right)\right. \\
&\left.-\left(\prod_{p=1}^{L+1}\mathbf{A}^{(p)}\right)\mathbf{B}^{(L+1)}\right\|_F \\
&= \left\|\sum_{p=0}^{L}\left(\prod_{q=1}^{p}\mathbf{A}^{(q)}\right)\left(\mathbf{B}^{(p)}-\mathbf{A}^{(p+1)}\mathbf{B}^{(p+1)}\right)\right\|_F.
\end{aligned} \tag{22}$$

Due to the triangle inequality of a matrix norm [12], we have

$$\left\|\mathbf{B}^{(0)}-\left(\prod_{p=1}^{L+1}\mathbf{A}^{(p)}\right)\mathbf{B}^{(L+1)}\right\|_F \leq \sum_{p=0}^{L}\left\|\left(\prod_{q=1}^{p}\mathbf{A}^{(q)}\right)\left(\mathbf{B}^{(p)}-\mathbf{A}^{(p+1)}\mathbf{B}^{(p+1)}\right)\right\|_F. \quad (23)$$

From Fig. 1, it can be clearly seen that the sparsity pattern of $\mathbf{A}^{(p+1)}\mathbf{B}^{(p+1)}$ is equal to that of $\mathbf{B}^{(p)}$. It is because they are essentially the same matrices. The only difference is that the blocks of $\mathbf{B}^{(p)}$ are vertically split and then compressed by the ACA-SVD to obtain $\mathbf{A}^{(p+1)}\mathbf{B}^{(p+1)}$. Furthermore, from Fig. 1, we also can conclude that the sparsity pattern of $\mathbf{A}^{(p+1)}\mathbf{M}$ is equal to that of $\mathbf{B}^{(p)}$, if the matrix $\mathbf{M}$ has the same sparsity pattern as $\mathbf{B}^{(p+1)}$. By recursively applying this conclusion, we can find that both $\left(\prod_{q=n+1}^{p}\mathbf{A}^{(q)}\right)\mathbf{B}^{(p)}$ and $\left(\prod_{q=n+1}^{p+1}\mathbf{A}^{(q)}\right)\mathbf{B}^{(p+1)}$ have the same sparsity pattern as $\mathbf{B}^{(n)}$ for $1\leq n\leq p$. Thus

$$\left(\prod_{q=n+1}^{p}\mathbf{A}^{(q)}\right)\left(\mathbf{B}^{(p)}-\mathbf{A}^{(p+1)}\mathbf{B}^{(p+1)}\right) = \left(\prod_{q=n+1}^{p}\mathbf{A}^{(q)}\right)\mathbf{B}^{(p)}-\left(\prod_{q=n+1}^{p+1}\mathbf{A}^{(q)}\right)\mathbf{B}^{(p+1)} \quad (24)$$

also has the same sparsity pattern as $\mathbf{B}^{(n)}$. Due to Corollary 1, we find

$$\begin{aligned}&\left\|\left(\prod_{q=1}^{p}\mathbf{A}^{(q)}\right)\left(\mathbf{B}^{(p)}-\mathbf{A}^{(p+1)}\mathbf{B}^{(p+1)}\right)\right\|_F\\ &=\left\|\left(\prod_{q=2}^{p}\mathbf{A}^{(q)}\right)\left(\mathbf{B}^{(p)}-\mathbf{A}^{(p+1)}\mathbf{B}^{(p+1)}\right)\right\|_F\\ &=\left\|\left(\prod_{q=3}^{p}\mathbf{A}^{(q)}\right)\left(\mathbf{B}^{(p)}-\mathbf{A}^{(p+1)}\mathbf{B}^{(p+1)}\right)\right\|_F\\ &\cdots\\ &=\left\|\mathbf{A}^{(p)}\left(\mathbf{B}^{(p)}-\mathbf{A}^{(p+1)}\mathbf{B}^{(p+1)}\right)\right\|_F\\ &=\left\|\mathbf{B}^{(p)}-\mathbf{A}^{(p+1)}\mathbf{B}^{(p+1)}\right\|_F. \end{aligned} \quad (25)$$

Substituting (25) into (23) and using Lemma 1, we obtain

$$\left\|\mathbf{B}^{(0)}-\left(\prod_{p=1}^{L+1}\mathbf{A}^{(p)}\right)\mathbf{B}^{(L+1)}\right\|_F \leq \sum_{p=0}^{L}\left\|\mathbf{B}^{(p)}-\mathbf{A}^{(p+1)}\mathbf{B}^{(p+1)}\right\|_F \leq \varepsilon\sum_{p=0}^{L}\left\|\mathbf{B}^{(p)}\right\|_F. \quad (26)$$

Then, substituting (26) into (3), the relative Frobenius norm error of the MLACA satisfies

$$\frac{\left\|\mathbf{B}^{(0)}-\left(\prod_{p=1}^{L+1}\mathbf{A}^{(p)}\right)\mathbf{B}^{(L+1)}\right\|_F}{\left\|\mathbf{B}^{(0)}\right\|_F} \leq \varepsilon\sum_{p=0}^{L}\frac{\left\|\mathbf{B}^{(p)}\right\|_F}{\left\|\mathbf{B}^{(0)}\right\|_F}. \quad (27)$$

If $p=0$, $\left\|\mathbf{B}^{(p)}\right\|_F/\left\|\mathbf{B}^{(0)}\right\|_F=1$. If $1\leq p\leq L$, $\left\|\mathbf{B}^{(p)}\right\|_F/\left\|\mathbf{B}^{(0)}\right\|_F$ can be rewritten as

$$\frac{\left\|\mathbf{B}^{(p)}\right\|_F}{\left\|\mathbf{B}^{(0)}\right\|_F}=\frac{\left\|\mathbf{B}^{(1)}\right\|_F}{\left\|\mathbf{B}^{(0)}\right\|_F}\frac{\left\|\mathbf{B}^{(2)}\right\|_F}{\left\|\mathbf{B}^{(1)}\right\|_F}\cdots\frac{\left\|\mathbf{B}^{(p)}\right\|_F}{\left\|\mathbf{B}^{(p-1)}\right\|_F}=\prod_{q=0}^{p-1}\frac{\left\|\mathbf{B}^{(q+1)}\right\|_F}{\left\|\mathbf{B}^{(q)}\right\|_F}. \quad (28)$$

According to Lemma 3, this yields

$$\frac{\left\|\mathbf{B}^{(p)}\right\|_F}{\left\|\mathbf{B}^{(0)}\right\|_F}\leq(1+\varepsilon)^p. \quad (29)$$

for $0\leq p\leq L$.

Finally, substituting (29) into (27), we obtain

$$\frac{\left\|\mathbf{B}^{(0)}-\left(\prod_{p=1}^{L+1}\mathbf{A}^{(p)}\right)\mathbf{B}^{(L+1)}\right\|_F}{\left\|\mathbf{B}^{(0)}\right\|_F} \leq \varepsilon\sum_{p=0}^{L}(1+\varepsilon)^p=(1+\varepsilon)^{L+1}-1. \quad (30)$$

Equation (30) states that for the L-level MLACA, which includes $L+1$ steps and compresses $\mathbf{B}^{(0)}$ into a product of $L+2$ sparse matrices, the relative Frobenius norm error is not larger than $(1+\varepsilon)^{L+1}-1$, where ε is the relative Frobenius norm error of the ACA-SVD used in the MLACA. In consequence, if we set the threshold of the ACA-SVD to $(1+\varepsilon)^{\frac{1}{L+1}}-1$, it is guaranteed that the error of the L-level MLACA is smaller than ε for any L. In practical applications, ε is always $\ll 1$. Thus, we can approximate $(1+\varepsilon)^{L+1}-1$ with $\varepsilon(L+1)$ as the error bound of the MLACA.

III. Conclusion

In this communication, an error upper bound of the MLACA for compressing a MoM impedance submatrix associated with two well-separated blocks has been rigorously derived. If the relative Frobenius norm error of the ACA-SVD used in the MLACA is not larger than ε, the proof shows that the relative Frobenius norm error of the L-level MLACA does not exceed $(1+\varepsilon)^{L+1}-1$. The error bound can be approximated as $\varepsilon(L+1)$, because $\varepsilon\ll 1$ for practical applications. Thanks to this error upper bound, the error of the MLACA can be easily controlled.

References

[1] M. Bebendorf, "Approximation of bound element matrices," *Numer. Math.*, vol. 86, no. 4, pp. 565–589, 2000.

[2] K. Zhao, M. N. Vouvakis, and J.-F. Lee, "The adaptive cross approximation algorithm for accelerated method of moments computations of EMC," *IEEE Trans. Electromagn. Compat.*, vol. 47, no. 4, pp. 763–773, Nov. 2005.

[3] M. Bebendorf and S. Kunis, "Recompression techniques for adaptive cross approximation," *J. Integ. Equ. Appl.*, vol. 21, no. 3, pp. 331–357, 2009.

[4] A. Heldring, J. M. Rius, J. M. Tamayo, J. Parrón, and E. Ubeda, "Multiscale compressed block decomposition for fast direct solution of method of moments linear system," *IEEE Trans. Antennas Propag.*, vol. 59, no. 2, pp. 526–536, Feb. 2011.

[5] J. M. Tamayo, A. Heldring, and J. M. Rius, "Multilevel adaptive cross approximation (MLACA)," *IEEE Trans. Antennas Propag.*, vol. 59, no. 12, pp. 4600–4608, Dec. 2011.

[6] A. Heldring, J. M. Tamayo, C. Simon, E. Ubeda, and J. M. Rius, "Sparsified adaptive cross approximation algorithm for accelerated method of moments computations," *IEEE Trans. Antennas Propag.*, vol. 61, no. 1, pp. 240–246, Jan. 2013.

[7] X. Chen, C. Gu, Z. Niu, and Z. Li, "Fast adaptive cross-sampling scheme for the sparsified adaptive cross approximation," *IEEE Antennas Wireless Propag. Lett.*, vol. 13, pp. 1061–1064, Jun. 2014.

[8] X. Chen, C. Gu, Z. Li, and Z. Niu, "Sparsified multilevel adaptive cross approximation," in *Proc. 3rd IEEE Asia-Pac. Conf. Antennas Propag. (APCAP'14)*, Jul. 2014, pp. 971–973.
[9] X. Chen, C. Gu, J. Ding, Z. Li, and Z. Niu, "Multilevel fast adaptive cross-approximation algorithm with characteristic basis functions," *IEEE Trans. Antennas Propag.*, vol. 63, no. 9, pp. 3994–4002, Sep. 2015.
[10] W. C. Gibson, *The Method of Moments in Electromagnetics*. Boca Raton, FL, USA: CRC Press, 2007.
[11] E. Michielssen and A. Boag, "A multilevel matrix decomposition algorithm for analyzing scattering from large structures," *IEEE Trans. Antennas Propag.*, vol. 44, no. 8, pp. 1086–1093, Aug. 1996.
[12] G. H. Golub and C. F. Van Loan. *Matrix Computations*. Baltimore, MD, USA: The Johns Hopkins Univ. Press, 1996.

Broadband Reflectarray Antenna Using Subwavelength Elements Based on Double Square Meander-Line Rings

Pei-Yuan Qin, Y. Jay Guo, and Andrew R. Weily

***Abstract*—A linearly polarized broadband reflectarray is presented employing a novel single layer subwavelength phase shifting element. The size of the element is a fifth of a wavelength at the center frequency of 10 GHz and the element consists of double concentric square rings of meander lines. By changing the length of the meander line, a 420° phase variation range is achieved at the center frequency. This characteristic makes the proposed configuration unique, as most of the reported subwavelength reflectarray elements can only realize a phase range far less than 360°. In addition, the slope of the phase response remains almost constant from 9 to 11 GHz, demonstrating a broadband property. A 48 × 48-element reflectarray antenna is simulated, fabricated, and measured. Good agreement is obtained between simulated and measured results. A measured 1.5-dB gain bandwidth of 18% and 56.5% aperture efficiency is achieved.**

***Index Terms*—Double square ring, meander line, microstrip, reflectarray antenna, subwavelength.**

I. Introduction

A reflectarray antenna consists of an array of phase shifting elements on a flat surface that provide an appropriate phase response to form a focused beam or a contoured beam when illuminated by a feed [1]–[5]. Due to their advantages of low profile, light weight, and ease of transportation, reflectarray antennas have become attractive for satellite communication systems. Compared to their parabolic reflector counterparts, however, reflectarrays tend to have narrower bandwidth that limits their practical applications. This is partly due to the inherent narrow band property of most phase shifting elements. In order to overcome this drawback, several techniques have been proposed such as using stacked phase shifting elements [6] or patches aperture coupled to true-time delay lines [7]. In order to reduce the manufacturing cost and mitigate the alignment errors that occur in multilayer reflectarrays, single-layer broadband reflectarrays have been proposed, which employ multiresonant elements, such as double circular/square rings [8], [9] or circular rings with open-circuited stubs [10].

Recently, in contrast to the aforementioned reflectarray elements with a cell size of half a wavelength, subwavelength coupled-resonant elements were introduced [11]–[15], where the resonance is a result of the coupling between the elements instead of the self resonance of the elements. The reflectarray made from subwavelength elements can achieve a higher gain compared to its counterparts with half-wavelength elements [12]. However, there are some limitations for the currently reported subwavelength elements. First, the achievable phase range is usually much smaller than 360° partly due to the etching tolerance on the small gaps between the elements and it decreases significantly with the cell size. Take, e.g., a normal chemical etching process with a tolerance of 0.1–0.2 mm, a single-layer rectangular patch element with an element size of $\lambda/3$ has a phase range around 300° [12], [13]. As a result, there is always an unattainable phase range that will result in phase errors and reduce the antenna gain. Such drawbacks are more severe for subwavelength elements with a size smaller than $\lambda/3$. Second, when calculating the phase response of a reflectarray cell element, the mutual coupling effects are generally taken into account by assuming all its surrounding elements are the same in an infinite periodic environment. However, for subwavelength variable-sized elements, such an approach may lead to inaccuracies.

In this communication, a single-layer phase shifting element with a cell size of $\lambda/5$ at 10 GHz based on double square meander-line microstrip rings is proposed. By varying the length of the meander line, a phase variation range of around 420° can be obtained. In addition, as the size variation range of the proposed element is much smaller than other reported subwavelength elements, the mutual coupling effects can be analyzed more accurately. A 48×48-element reflectarray operating at 10 GHz is designed to validate the performance of the proposed element. The 1.5-dB gain bandwidth is found to be 18% and the 3-dB bandwidth is greater than 32%. The proposed wideband reflectarray is suitable for satellite communications, such as DBS systems, with appropriate scaling of the operating frequency.

Compared to our previous design on a phase shifting element using similar double square meander-line rings, which could only realize a 340° phase range, this communication extends the work reported in [16] significantly and the main contribution is as follows. First, a new single-layer subwavelength cell element is proposed that can satisfy the 360° phase range requirement and has wideband performance. Second, the operating mechanism of the phase shifting element and the design method are described. Third, the simulated and measured results for a complete reflectarray antenna are shown, which validates the feasibility of the proposed cell element.

This communication is organized as follows. In Section II, the configuration of the proposed phase shifting element is described and the simulated phase responses are provided. Its operating mechanism is investigated in Section III by using parametric studies. Then, the design of the reflectarray is presented in Section IV. Finally, the conclusion is given in Section V.

II. Phase Shifting Element

Fig. 1 shows the configuration of the reflectarray element. It is composed of two concentric square meander-line microstrip rings and is designed on a 3.175-mm-thick RO5880 substrate (dielectric constant

Manuscript received April 25, 2015; revised November 06, 2015; accepted November 18, 2015. Date of publication November 23, 2015; date of current version December 31, 2015.

P.-Y. Qin and Y. J. Guo are with the Faculty of Engineering and Information Technology, University of Technology, Sydney, N.S.W. 2007, Australia.

A. R. Weily is with the Data61, CSIRO, Sydney, N.S.W. 1710, Australia.

Color versions of one or more of the figures in this communication are available online at http://ieeexplore.ieee.org.

Digital Object Identifier 10.1109/TAP.2015.2502978